

pubs.acs.org/acscatalysis Research Article

Adsorption Energies of Oxygenated Aromatics and Organics on Rhodium and Platinum in Aqueous Phase

James Akinola, Isaiah Barth, Bryan R. Goldsmith,* and Nirala Singh*



Cite This: ACS Catal. 2020, 10, 4929-4941



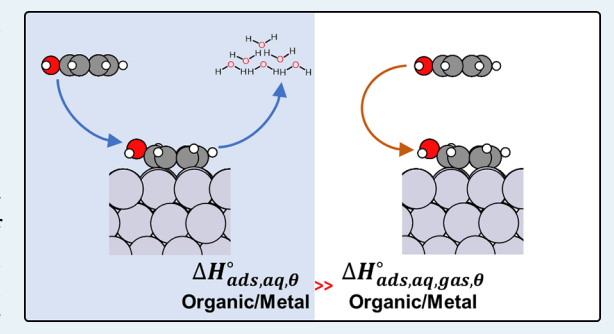
ACCESS

III Metrics & More

Article Recommendations

Supporting Information

ABSTRACT: Accurately predicting adsorption energies of oxygenated aromatic and organic molecules on metal catalysts in the aqueous phase is challenging despite its relevance to many catalytic reactions such as biomass hydrogenation and hydrodeoxygenation. Here, we report the aqueous-phase adsorption enthalpies and free energies of phenol, benzaldehyde, furfural, benzyl alcohol, and cyclohexanol on polycrystalline Pt and Rh determined via experimental isotherms and density functional theory modeling. The experimental aqueous heats of adsorption for all organics are ~50 to 250 kJ mol⁻¹ lower than calculated gas-phase heats of adsorption, with a larger decrease for Rh compared with that for Pt. Unlike in gas phase, phenol and other aromatic organics adsorb with similar strength on Pt and Rh in aqueous



phase. The similar aqueous adsorption strength of phenol and benzaldehyde on Pt and Rh explains their comparable aqueous-phase hydrogenation activities, which are rate-limited by a Langmuir—Hinshelwood surface reaction. A widely used implicit solvation model largely overpredicts the heats of adsorption for all organics compared with experimental measurements. However, accounting for the enthalpic penalty of displacing multiple water molecules upon organic adsorption using a bond-additivity model gives a much closer agreement between experimental measurements and predicted heats of adsorption. This bond-additivity model explains that the similar adsorption strength of organics on Pt and Rh in aqueous phase is due to the stronger adhesion of water to Rh than that on Pt, which offsets the stronger gas-phase organic adsorption energy on Rh. The data reported herein also provides a valuable resource for benchmarking methods for predicting aqueous-phase adsorption energies of C5/C6 organics on metal surfaces.

KEYWORDS: adsorption energy, aqueous-phase adsorption, bond-additivity model, solvent effects, phenol, platinum, rhodium, cyclic voltammetry

■ INTRODUCTION

Over 143 billion gallons of motor gasoline are consumed annually within the United States to power transportation, emitting huge amounts of greenhouse gases like CO₂. The need to supply energy for transportation in a sustainable manner has spurred efforts to replace fossil fuels with renewable and CO2neutral transportation fuels. One promising strategy is to produce transportation fuels from lignin biomass waste.²⁻⁵ Converting the oxygenated aromatic compounds in water that come from fast pyrolysis of lignin (i.e., bio-oil) to transportation fuels or chemical precursors requires aqueous-phase catalytic or electrocatalytic hydrogenation and hydrodeoxygenation, o typically rate-limited on metals by surface reactions. To improve the kinetics of these and other aqueous-phase catalytic reactions, an understanding of the effect of water (or solvent) on organic adsorption is critical because adsorption energies can determine coverages and alter activation barriers.

Although adsorption energies on metals are generally well understood in the gas phase and have been used effectively to predict and understand gas-phase catalytic behavior, much less is known about adsorption in the aqueous phase. Generally, the lack of understanding of aqueous-phase adsorption can lead to inaccurate predictions of aqueous-phase catalytic behavior. This issue often occurs when gas-phase adsorption energies are used to explain aqueous-phase catalytic activity trends. For example, the experimental gas-phase adsorption of phenol (a model biooil species) on Pt(111) is so strong (-220 kJ mol⁻¹)⁷ that room-temperature hydrogenation would seem unlikely to occur because of site poisoning by phenol, yet phenol hydrogenation on Pt occurs in the aqueous phase at room temperature. ⁸⁻¹² Also, Pt(111) and Rh(111) are predicted by density functional theory (DFT) modeling to have a ~50 kJ mol⁻¹ difference in their adsorption energy of phenol in the gas phase, ¹³ but have similar aqueous-phase hydrogenation turnover frequencies (TOFs) and apparent activation barriers, ^{8,14} seemingly in

Received: February 17, 2020 Revised: March 29, 2020 Published: March 31, 2020





contradiction to the Sabatier principle. It is important to determine whether this contradiction is due to intrinsic differences in the mechanism and pathways of gas-phase vs aqueous-phase catalytic reactions or can be explained by the differences in effective adsorption energies in gas and aqueous phases.

In this work, we report adsorption enthalpies and free energies on Pt and Rh for select U.S. Department of Energy platform chemicals that serve as bio-oil model compounds. Specifically, phenol, benzaldehyde, and furfural, 15 as well as two hydrogenated products—benzyl alcohol and cyclohexanol—in aqueous phase on active hydrogenation electrocatalysts, Rh and Pt, are studied using cyclic voltammetry (CV) and DFT modeling. We show the first direct comparison of DFT-computed adsorption energies with experimentally extracted values for these molecules and surfaces in the aqueous phase. We also show that the initial apparent discrepancies in the catalytic behavior of phenol and benzaldehyde hydrogenation in the aqueous phase can be explained by the stark differences in gasphase and aqueous-phase adsorption energies.

Adsorption of reactants in the condensed phase is more complex than in the gas phase because it requires displacement of adsorbed solvent before reactants can adsorb. To accurately describe surface reactions at liquid—solid interfaces, the energy of water/solvent displacement on the adsorption energetics of adsorbates must be adequately captured. The current first-principles modeling paradigm (i.e., using DFT) for predicting adsorption energies and coverages to use in microkinetic models typically neglect the energetic cost of displacing adsorbed solvent from the catalyst surface. Because adsorption energies play such a significant role in catalytic activity, these errors could qualitatively change predicted trends in catalyst performance.

Recent work shows that the aqueous-phase heat of adsorption of phenol on a Pt(111)-like surface is much smaller than the gas phase, ¹⁶ which was attributed to the enthalpy associated with the displacement of multiple water molecules from the Pt surface upon adsorption of phenol and described by a bond-additivity model. ¹⁷ This more moderate adsorption energy of phenol is consistent with the aqueous-phase electrocatalytic and thermocatalytic hydrogenation activities observed at room temperature. Nonetheless, the aqueous-phase heats of adsorption and the role of water displacement on metals are unknown for most other oxygenated aromatic and organic species of relevance to bio-oil catalysis. This lack of knowledge prevents understanding of how the adsorption strength of reactants correlates with catalytic activity in the aqueous phase and also precludes important benchmarking of computational predictions.

In this work, we (1) apply a state-of-the-art bond-additivity model to five molecules on Pt(111) terraces, Pt(110) steps, Rh(111) terraces, and Rh(110) steps; (2) confirm that the adsorption of these molecules is reversible, which is a requirement for extracting adsorption energies using adsorption isotherms; and (3) perform a DFT analysis for all studied molecules to compare adsorption energies quantitatively with our experimental measurements. We show that these DFT-computed adsorption energies can be directly compared with experimentally extracted values for these molecules and surfaces in the aqueous phase. Each of these three aspects improves upon previous investigations and taken together provides a more advanced study of molecule adsorption in the aqueous phase than prior work.

We use CV to measure the charge from reversible hydrogen underpotential deposition (H_{upd}) and desorption $(H^+ + e^- +$

(Metal) \rightleftarrows H)^{19–21} on polycrystalline Rh and Pt without organics present and with increasing organic concentration. The decrease in $H_{\rm upd}$ charge due to adsorbed organics^{11,22–24} is used to estimate the organic coverage as a function of organic concentration and construct adsorption isotherms. Aqueousphase adsorption equilibrium constants are extracted using a Temkin adsorption model to fit the adsorption isotherms. Enthalpies are determined from the Gibbs free energies of adsorption as previously described. Adsorption enthalpies and free energies of these organics on Pt and Rh surfaces are also predicted using DFT modeling and a bond-additivity model to compare with experimental values.

Ultimately, our work finds that the heats of adsorption of organics in the aqueous phase are reduced by 50–250 kJ mol⁻¹ compared with their gas-phase values because of the enthalpic penalty of displacing several water molecules upon adsorption. This weaker adsorption explains why surface reactions of organics that bind too strongly to react in the gas phase can occur at room temperature in water. Additionally, we show that, unlike in gas phase, Rh and Pt have similar adsorption energies in aqueous phase for phenol, benzaldehyde, and their reaction intermediates. This similar adsorption energy in aqueous phase could be responsible for the comparable aqueous catalytic hydrogenation activity of these model bio-oil compounds observed on Pt and Rh. We also show that using DFT modeling with only implicit solvation overestimates adsorption energies and does not capture observed experimental trends, which prevents accurate predictions of coverages. Using a bondadditivity model combined with gas-phase DFT calculations enables more accurate predictions of aqueous adsorption energies of C5/C6 organics. These results highlight the necessity of properly accounting for the effect of solvent displacement at the metal interface when modeling the adsorption of organic molecules of relevance to condensedphase catalytic reactions such as bio-oil hydrogenation, particularly those with large adsorption footprints such as

EXPERIMENTAL AND COMPUTATIONAL METHODS

Cyclic Voltammetry. The working electrode for the CV measurements was either a polycrystalline Pt wire (0.5 mm diameter, 99.997% Alfa Aesar) or Rh wire (0.5 mm diameter, 99.8% Alfa Aesar), and the counter electrode was a graphite rod. A two-compartment electrochemical cell with a working and reference electrode compartment and a counter electrode compartment separated by an N117 Nafion membrane was used. The working electrodes were first exposed to a flame for cleaning any adventitious organic, followed by rinsing with Milli-Q water. Before each use, the cell was cleaned with Milli-Q water and oven-dried at 80 °C three times. This cleaning procedure removes trace impurities of organics that would otherwise result in inconsistent measurements from run to run. A Ag/AgCl reference electrode was calibrated to 0 V vs reversible hydrogen electrode (RHE) in the supporting electrolyte, and all potentials are reported vs RHE based on this calibration. Acetate buffer (pH 5) containing 100 mM acetic acid (Sigma-Aldrich, 99.995%) and 100 mM sodium acetate (Sigma-Aldrich, 99.999%) was used as the supporting electrolyte. Acetic acid is used in this work to mimic a bio-oil environment containing carboxylic acids 25 and has negligible adsorption on Pt and Rh in the $\,H_{upd}$ region. $^{26}\,$ The working electrode compartment was filled with 130 mL of acetate buffer and sparged with N₂

(99.999%) to remove dissolved oxygen. The working electrode was further cleaned under voltammetric conditions in the potential window of $-0.2-1.8~\rm V$ vs RHE for 60 cycles at a scan rate of $100~\rm mV~s^{-1}$. After voltammetric cleaning, CV was carried out at a $100~\rm mV~s^{-1}$ scan rate in the potential window of $0.05-1.1~\rm V$ for Rh wire and $0.05-1.3~\rm V$ for Pt wire. Within these potential windows, the cyclic voltammograms were repeatable and reversible. There was no scan rate dependence (between 20 and $100~\rm mV~s^{-1})$ of the $H_{\rm upd}$ charge on Pt 16 and less than 7% change in $H_{\rm upd}$ charge with scan rate on Rh (Figure S1 and Table S1).

Organics dissolved in acetate buffer solution were introduced to the cell to increase the concentration of organics from 1 μ M up to 500 mM. The organics used for adsorption studies were phenol (Sigma-Aldrich, >99%), benzaldehyde (Sigma-Aldrich, >99%), furfural (Sigma-Aldrich, 99%), benzyl alcohol (Sigma-Aldrich, 99.8%), and cyclohexanol (Sigma-Aldrich, 99%). At the lowest organic concentration $(1 \mu M)$, the bulk organic concentration would decrease by at most 0.2% upon adsorption of a complete monolayer of the organic onto the metal electrode; thus, we assumed that the bulk concentration was unchanged by adsorption (see Section S2 of the Supporting Information (SI) for calculation details). The electrolyte was stirred and re-sparged with N2 to remove oxygen prior to CV measurements for each organic concentration. The working electrode was continuously cycled in the same potential window between each CV measurement (0.05-1.1 V for Rh and 0.05-1.3 V for Pt). The CV measurements were repeated under the conditions specified at each organic concentration until a steady state was reached. The charge from chemisorbed hydrogen in the H_{uvd} region (0.05 V-0.35 V) was obtained by integrating the area under the desorption peaks in the CV, dividing by the scan rate and then subtracting the baseline capacitive charge calculated from the double-layer charging region of the CV. With phenol present, the H_{upd} charge from H* adsorption and desorption matches closely on Pt (Figure S2a). On Rh, the H adsorption region had a contribution from the Rh₂O₃ reduction peak, 19 causing the apparent adsorption charge to be larger than the desorption charge (Figure S2b); hence, the H_{upd} desorption peak was used instead to estimate the amount of chemisorbed hydrogen on both Rh and Pt.

Dilution of Organic Concentration to Determine Reversibility. To test whether organic adsorption was reversible, after taking a cyclic voltammogram at a given organic concentration the organic concentration was diluted by removing a given volume of the existing solution and replacing with the same volume of acetate buffer supporting electrolyte, while the working electrode containing the adsorbed organic was kept in place under a continuous blanket of N_2 . After dilution, the working electrode was cycled at the normal potential window used for $H_{\rm upd}$ measurements until the adsorbed organic reached equilibrium with the diluted cell solution concentration (indicated by a stable CV). This stable CV at the diluted concentration was compared to measurements done at the same concentration, but without previously going to higher organic concentrations.

Adsorption Isotherm Fitting. Each isotherm was fit by a one-site or two-site model using the same procedure from ref 16. Briefly, the equilibrium constant of adsorption $K_{\rm eq,ads,\theta}^{\rm aq}$ for each site was obtained by fitting the fraction of $H_{\rm upd}$ inhibited at different organic concentrations to a Temkin isotherm (eq 1), where the saturation coverage for site 1 was the coverage (θ) where the first plateau is seen, and the saturation coverage of site

2 was the second plateau. $\Delta G_{\mathrm{ads,aq},\theta=0}^{\circ}$ is the adsorption free energy of the aqueous organic at zero coverage, R is the ideal gas constant, and T is the temperature. Several models can be used to fit the adsorption isotherm, such as the Langmuir-Hinshelwood (LH) model, where metal surface sites can either be unoccupied, have adsorbed hydrogen, or have adsorbed organic. Instead of an LH model, we used a modified Langmuir model where the organic adsorption energy varies linearly with the coverage because of adsorbate-adsorbate interactions (also known as the Temkin model). 27,28 The Temkin model assumes that the coverage of organic does not depend on the adsorbed H in the reversible H_{upd} region but depends only on the bulk organic concentration and the organic equilibrium adsorption constant. This model is used because of its simplicity compared to the LH model. Recently, an LH model was used to fit kinetics for Pt/C for aqueous-phase phenol hydrogenation over a range of phenol concentrations, resulting in an equilibrium constant for phenol of 33 (standard-state concentration of 1 M phenol, as used here).²⁹ This value is similar to the adsorption equilibrium constant of 38 measured for phenol/Pt(111) using the Temkin model, 16 supporting the accuracy of the Temkin model used for this work. Additional discussion about the isotherm derivation and fitting is provided in Section S6 of the SI.

$$K_{\text{eq,ads},\theta}^{\text{aq}} = \exp\left(-\frac{\Delta G_{\text{ads,aq},\theta=0}^{\circ} + \alpha\theta}{RT}\right)$$
 (1)

Ideally, the measurements would be done as a function of surface charge on both Pt and Rh to determine the influence of the surface charge of the metal electrode on the water layer and organic adsorption 30,31 or at a potential where the maximum organic adsorption is reached, often slightly cathodic to the potential of zero charge (PZC). However, the $H_{\rm upd}$ technique inherently cannot be done at a single potential but requires cycling over a range of potentials. Hence, our reported values may be underpredictions of the organic adsorption strength relative to the adsorption on an uncharged surface. Despite this, there is still a general agreement between the adsorption energies extracted through this method and solution calorimetry, as well as gas-phase calorimetry once the effects of the water layer on the metal surface have been accounted for. 17

Computational Methods. Density functional theory (DFT) calculations were done using the Vienna ab initio simulation package (VASP). 33,34 All DFT calculations were nonspin-polarized because spin polarization was found to have 0.14 and 0.43% average changes in the organic and water adsorption energies, respectively, on Pt and Rh in the gas phase. The Perdew-Burke-Ernzerhof functional with the semiempirical D3 dispersion correction (PBE-D3) was used because of its good trade-off between computational cost and accuracy, although PBE-D3 has been shown to overestimate the adsorption strengths of aromatics.^{35–38} Projector-augmented wave pseudopotentials³⁹ were used with a kinetic energy cutoff at 400 eV. The convergence criteria for electronic and ionic forces were set to 10⁻⁵ eV and 0.01 eV Å⁻¹. Atomic structures were geometry-optimized using either the conjugate-gradient algorithm or the quasi-Newton algorithm. Lattice parameters of bulk Pt and Rh were determined by relaxing a four-atom facecentered cubic cell of each metal. A $15 \times 15 \times 15$ Monkhorst– Pack k-point grid was used for bulk relaxations. The calculated lattice parameters were 3.925 and 3.792 Å for Pt and Rh and are within 1.2 and 0.1%, respectively, of the experimentally determined values. 40,41

The adsorption enthalpies of phenol, benzaldehyde, furfural, benzyl alcohol, and cyclohexanol were predicted on (111) terraces and the (110)-like and (100)-like steps of the (553) and (533) surfaces, respectively. Throughout this text, we refer to the steps of the (553) and (533) surfaces simply as (110) and (100), respectively. The surface slab models of Pt and Rh were modeled using 4×4 supercells that were four layers thick. For all considered surfaces, the top two layers could relax during geometry optimization, whereas the bottom two layers were fixed in their bulk coordinates. Metal slabs were separated by a 20 Å vacuum in the direction perpendicular to the surface. A 3 \times 3×1 Monkhorst-Pack k-point grid was used for adsorption energy calculations of organics on 4 × 4 slabs corresponding to a 1/16 monolayer (ML) coverage. A $5 \times 5 \times 1$ Monkhorst-Pack k-point grid was used for adsorption energy calculations of organics on 3×3 slabs corresponding to a 1/9 ML coverage. Spurious dipole interactions between periodic images were corrected in VASP (IDIPOL = 3, LDIPOL = true).

A variety of implicit and explicit modeling approaches have been used to treat the water—adsorbate—metal interface to enable the prediction of thermodynamic and kinetic parameters for aqueous-phase reactions. ⁴²,43 Explicit treatment of water through classical, ⁴⁴ ab initio, ⁴⁵ and hybrid ⁴⁶ molecular dynamics calculations has been employed to describe water—adsorbate—metal interactions at the interface, although these approaches are computationally demanding because they require sampling over long time scales. Alternatively, simple ice-like layers have been used to explicitly model water, although this approach is too crude to accurately describe the water—adsorbate—metal interactions at standard electrochemical conditions. ⁴⁴ In place of explicit solvent modeling, adsorption energies may be calculated using computationally inexpensive implicit solvent models. ^{47,48}

Two approaches, an implicit solvent model using the VASPsol model^{49,30} and a bond-additivity model recently published by Singh and Campbell,¹⁷ were used in this study to model solvation effects. VASPsol, which was developed to treat solvated molecules and nanocrystal surfaces, models the interactions between the solvent and solute by using DFT to describe the solute explicitly and the linear Poisson-Boltzmann equation to describe the solvent as a continuum dielectric. In this work, the water solvent was implicitly treated using the default VASPsol parameters (see Section S7 for gas-phase, implicit solvent, and thermodynamic calculations). The bondadditivity model, which accounts for the formation of waterorganic bonds as well as the breaking of water-water and water-metal bonds, was originally developed to estimate the aqueous-phase adsorption energy of phenol on Pt(111) based on the experimental gas-phase adsorption energy.

Here, the bond-additivity model $(eq 2)^{17}$ was used to estimate the aqueous-phase adsorption enthalpies of all organic molecules considered at 298.15 K and 1 atm.

$$-\Delta H_{\text{ads,aq,gas,R/M}}^{\circ} = -\Delta H_{\text{ads,gas,R/M}}^{\circ}$$

$$+ n(\Delta H_{\text{ads,gas,water/M}}^{\circ} + \Delta H_{\text{vap}}^{\circ})$$

$$- 2\gamma_{\text{water(lio)}}\sigma_{\text{R}} + (\text{water - R})$$
(2)

 $\Delta H_{\mathrm{ads,aq,gas,R/M}}^{\circ}$ is the adsorption enthalpy of gas-phase organic R onto metal M in the aqueous phase, $\Delta H_{\mathrm{ads,gas,R/M}}^{\circ}$ is the adsorption enthalpy of gas-phase organic R onto metal M in the gas phase, n is the number of water molecules displaced from metal M upon organic adsorption, $\Delta H_{\mathrm{ads,gas,water/M}}^{\circ}$ is the adsorption enthalpy of a water molecule onto metal M in the

gas phase, $\Delta H_{\mathrm{vap}}^{\circ}$ is the vaporization enthalpy of water, $\gamma_{\mathrm{water}(\mathrm{liq})}$ is the surface energy of liquid water, σ_{R} is the area of an adsorbed organic molecule, and water—R is $-1/2\Delta H_{\mathrm{Solv,R}} + \gamma_{\mathrm{water}(\mathrm{liq})}\sigma_{\mathrm{R}}$, where $\Delta H_{\mathrm{Solv,R}}$ is the solvation enthalpy of the organics in water. For simplicity, in the subsequent text, we omit R or R/M when it is clear which metal and organic are being referred to (e.g., we refer to $\Delta H_{\mathrm{ads,aq,gas,R/M}}^{\circ}$ as $\Delta H_{\mathrm{ads,aq,gas}}^{\circ}$). A similar equation using experimental adhesion energies (rather than our calculated values) of aqueous and nonaqueous solvents is presented in ref 51, but as the adhesion energy of water on Rh is not experimentally available, we use eq 2 here. Conceptually, these equations are the same bond-additivity model.

The number of water molecules displaced upon organic adsorption, n, was calculated for each molecule on each surface by studying the heat of adsorption as a function of organic coverage using the bond-additivity model (details provided in Section S11 of the Supporting Information). Treating each modeled coverage as saturation, n was calculated over a range of organic coverages. In subsequent applications of the bondadditivity model, we choose the n that corresponds to the coverage at which the heat of adsorption reaches a maximum. Using this method, we find that phenol adsorbs on Pt(111) at a 1/9 ML coverage (9 Pt atoms per phenol molecule) and displaces 6.5 water molecules assuming a water coverage of 0.72 ML. 52 This phenol coverage on Pt(111) matches the coverage in aqueous phase determined from quantitative Auger electron spectroscopy measurements,⁵³ and the value of 6.5 water molecules is the same as used in our previous bond-additivity model for phenol on Pt(111) using experimental values. Therefore, we believe that our computational approach is reasonable for estimating the number of water molecules displaced from the Pt(111) terrace upon adsorption of phenol, and we apply it to the other organics on Pt(111) and Rh(111)terraces. Because it is difficult to vary organic coverage on stepped surfaces, we calculate n on (110) and (100) terraces and assume that *n* is the same on the respective steps. Although the value of *n* on stepped surfaces may be evaluated more rigorously using ab initio molecular dynamics, this computationally demanding approach was not employed in this current work. Since n is not calculated explicitly on (110) and (100) steps, predicted heats of adsorption on the stepped surfaces are not as accurate as the heats of adsorption on the (111) terrace.

■ RESULTS AND DISCUSSION

Impact of Phenol on the Underpotential Deposition of **Hydrogen on Pt and Rh.** The data in Figure 1 shows that H_{und} on a Pt wire and a Rh wire is inhibited by phenol adsorption, which implies competitive adsorption between H* and phenol* on the surfaces of both metals in the aqueous phase. The cyclic voltammograms with phenol for the Pt wire (Figure 1a) match those measured previously, where the difference in H_{upd} charge on Pt with and without phenol was used to quantify the coverage of adsorbed phenol. $^{11,1\delta}$ On Rh, the $H_{\rm upd}$ charge, proportional to the H^* desorption peak area in the potential range of 0.05-0.35V, also decreases with increasing phenol concentration (H_{und} charge values are shown in Figure S2). Similar to Pt, we attribute the decreasing H_{upd} charge to the blocking of Rh sites by adsorbed phenol, resulting in fewer sites available for hydrogen to adsorb. Hydrogen underpotential deposition on Rh in acetate buffer without phenol is kinetically fast and reversible within the potential window used in this work, shown by the symmetry of the reduction and oxidation peaks associated with H_{upd} and the H_{upd} charge independence on scan rate (Figure S1 and Table

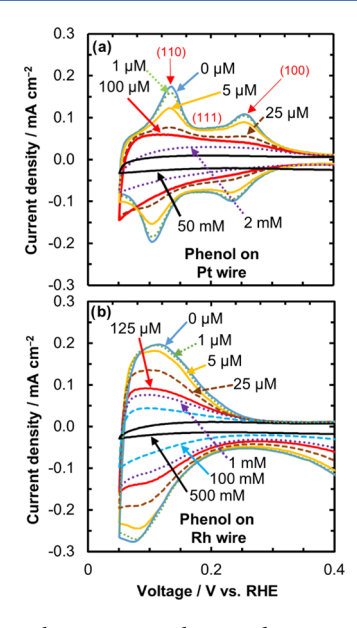


Figure 1. Cyclic voltammograms showing the H_{upd} region at different bulk phenol concentrations on (a) platinum wire and (b) rhodium wire. The H_{upd} current peaks attributed to Pt(110) steps and Pt(100) steps and the broad region corresponding to Pt(111) terraces are labeled. The H_{upd} peaks corresponding to different Rh facets overlap with one another. The cyclic voltammograms were taken in a 100 mM acetate buffer supporting electrolyte (pH 5) at 298 K and using a 100 mV s⁻¹ scan rate. Phenol competes with H^* adatoms for metal sites, hence the drop in area under the H_{upd} adsorption and desorption peaks as phenol concentration increases.

S1). The H_{upd} on Rh and Pt is also reversible when phenol is present (Figure S2), indicating that H* does not react with adsorbed phenol during these scans. The change in H_{upd} charge with phenol concentration is reproducible (Figure S3 and Table S2).

The polycrystalline Pt and Rh wires have different H_{upd} peak shapes, based on how H* interacts with the different surface facets. The peak voltages for Pt in Figure 1a are consistent with prior polycrystalline Pt studies, 11,16 and individual H_{upd} peaks have been identified on Pt single crystals in 0.1 M H₂SO₄ and HClO₄. ^{24,54} These studies indicate that the peak located at \sim 0.10 to 0.15 V is from Pt(110) steps, the peak at \sim 0.23 to 0.3 V is from Pt(100) steps, and the broad feature that underlies the two peaks from ~0.05 to 0.35 V is from Pt(111) terraces. Contributions from H_{upd} on (111) steps, (110) terraces, and (100) terraces on Pt are at CV peak locations that overlap with those of (111) terraces, (110) steps, and (100) steps.⁵⁵ Unlike on Pt, the H_{upd} peaks all overlap for the facets of polycrystalline Rh¹⁹ (i.e., Rh(110),⁶⁰ Rh(100),⁶¹ and $Rh(111)^{61-63}$). Consequently, a single adsorption/desorption peak is observed for H_{upd} on Rh wire in 0.1 M acetate buffer, Figure 1b. This overlap of H_{upd} peaks from the different facets of Rh, attributed to the similar hydrogen adsorption free energies on the different facets, makes deconvolution of organic adsorption on the different facets from $H_{\rm upd}$ alone difficult.

Adsorbed phenol blocks H_{upd} across the Pt facets to different extents, with the Pt(110) peak decreasing more than the Pt(100) peak for the same phenol concentrations, whereas the broad Pt(111) feature drops the least at concentrations between 1 and 100 μ M (Figure 1a). Therefore, the Pt(110) and Pt(100) steps adsorb phenol stronger than the Pt(111) terrace, in agreement with a prior report. ¹⁶ In Figure 1b, any differences in

phenol adsorption on the different facets of Rh wire are not immediately evident since the $H_{\rm upd}$ peaks of Rh(110), Rh(100), and Rh(111) cannot be distinguished. Nonetheless, we will show below based on the shape of the adsorption isotherm that there are also two distinct types of adsorption sites on Rh.

First, the inhibition of H_{upd} charge as a function of phenol concentration (Figure 1) can be used to extract adsorption energies using an adsorption isotherm, so long as the H_{upd} process remains reversible in the presence of phenol and phenol adsorption is an equilibrated, reversible process. We show that the H_{upd} oxidation and reduction charges match both in the absence of phenol and with phenol present (Figure S2), proving reversible H+ reduction and H* oxidation. This observation matches the report that phenol is reduced on Pt and Rh only at lower potentials (<0 V vs RHE) than applied in this work. To test whether the adsorption of organics on Pt and Rh is reversible, we measure the H_{upd} charge at a certain bulk organic concentration and then dilute the bulk concentration to see if the H_{und} charge recovers to that associated with the new (lower) bulk organic concentration (Figure S4). The observation that H_{upd} charge and thus phenol coverage are recovered (Table S3), i.e., there is no hysteresis in the adsorption isotherms, implies that phenol adsorption is an equilibrated, reversible process. The data in Figure S4 show that other organics also adsorb/desorb reversibly on both Pt and Rh.

Extracted Adsorption Energies of Phenol on Platinum and Rhodium. Having fulfilled both criteria for reversibility as discussed above, the adsorption isotherms of phenol on Pt and Rh shown in Figure 2 were constructed by plotting the fraction of H_{upd} inhibited by phenol from the cyclic voltammograms (Figure 1) against the bulk concentration of phenol. The fraction of H_{upd} inhibited, which we assume was caused by the reversible adsorption of phenol on the metal surface, was obtained from the difference in the H_{upd} charge with and without phenol in solution (details in Section S5 of the SI). The fraction of H_{upd} inhibited by phenol on Pt at different concentrations determined using the CV technique matches a report using a radiotracer method.⁶⁴ The dilution points are shown in Figure 2 as open triangles to indicate the reversibility of phenol adsorption and the lack of hysteresis using this technique. For example, diluting from 100 μ M (filled triangle) to 10 μ M (open triangle) is shown in the isotherm in Figure 2a for phenol on Pt wire, where the diluted point matches the measurement at 10 μ M without dilution. The variation between the data points after dilution compared to without dilution at the same bulk phenol concentration is within the small run-to-run variation from multiple measurements (see Figure S3 for run-to-run variations).

The isotherm shapes in Figure 2 indicate the presence of two distinct adsorption sites on both Pt and Rh, based on the initial increase in coverage with concentration, followed by a plateau with increasing concentration (saturation of the first site) and then by a second region of increasing coverage corresponding to adsorption on the second set of sites. Thus, we divide the phenol adsorption isotherm into two sites for both Pt and Rh, where site 1 corresponds to the stronger binding site and site 2 corresponds to the weaker binding sites. The $H_{\rm upd}$ peaks for Pt(110) and Pt(100) in Figure 1a decrease at lower phenol concentrations, whereas the Pt(111) $H_{\rm upd}$ peak only decreases at higher concentrations. Thus, site 1 in Figure 2a is attributed to a combination of stepped facets of Pt(110) and Pt(100), and site 2 is attributed to Pt(111) terraces. The adsorption free energy extracted in this way on site 2 matches those from a kinetic

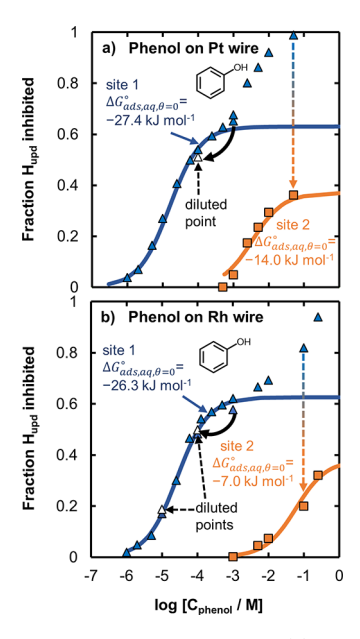


Figure 2. Adsorption isotherms of phenol on (a) Pt and (b) Rh wires constructed by plotting the fraction of H_{upd} inhibited by phenol vs the bulk phenol concentration. Each data point (blue triangle) is obtained from the drop in H_{upd} charge with phenol in **Figure 1**. Fits are from a two-site Temkin adsorption model with $\alpha=0$ kJ mol $^{-1}$ giving the best fit. The orange squares (site 2) correspond to the fraction of H_{upd} inhibited that is greater than the saturation amount of site 1. Thus, site 2 data points are adjusted by subtracting the saturation fraction of site 1 at the higher phenol concentration. Diluted points are shown by open triangles (solid black arrow indicates dilution by a factor of 10). The agreement of the diluted points with points directly taken by adding phenol without first reaching a higher concentration shows that phenol adsorption under these conditions is reversible.

model for phenol hydrogenation, as discussed in the Experimental and Computational Methods section. The fraction of site 2 corresponding to the Pt(111) terrace-like sites (0.37 from the isotherm for Pt in Figure 2 and 0.4 from ref 15) is similar to predictions from the electrochemical Wulff construction of the fraction of (111) sites (\sim 0.4 in the 0–0.4 V vs RHE range for Pt),65 supporting this assignment. Our DFT calculations using the bond-additivity model for Pt also predict stronger phenol adsorption on the (110) steps compared with that on the (111) terraces, consistent with our assignment. The model, however, predicts weaker phenol adsorption on the (100) steps than that on (111) terrace despite stronger adsorption in the gas phase. This discrepancy from the experimental results may be a result of an inaccurate (too strong) water adsorption energy on the (100) step or an inaccurate number of water molecules displaced upon organic adsorption, as discussed in the Experimental and Computational Methods section.

Although from the CV of Rh (Figure 1b) we cannot distinguish between facets, from Figure 2b it is apparent that there are two adsorption sites, where site 1 reaches saturation coverage at 1 mM phenol, followed by continued adsorption on site 2 at higher concentration. We attribute site 1 to a combination of (110) and (100) step facets and site 2 to (111) terraces, the same as the assignment on Pt. Our assignment is supported by a similar fraction of site 1 on Pt and Rh (0.63 and 0.62, respectively). The bond-additivity calculations for Rh predict that phenol adsorbs the strongest on (110) steps, followed by (111) terraces, and then the weakest on (100) steps, the same order as that predicted for Pt. It is possible that site 1 of Rh is only the (110) step and not the (100) steps, although the weak adsorption predicted on the (100) steps may

Table 1. Measured Adsorption Free Energies and Enthalpies of Organic Compounds on Rh and Pt Wires at 298 K in Aqueous Phase from Hydrogen Site-Blocking Experiments^a

molecule	$\Delta G_{ m ads,aq, heta=0}^\circ$	α	Sat. frac.	$-\Delta H_{ m ads,aq, heta}^{\circ}$	$-\Delta H_{ m ads,aq,gas, heta}^\circ$	$-\Delta H_{ m ads,aq,gas, heta}^{\circ}$
	$(kJ mol^{-1})^{b}$	$(kJ mol^{-1})$		$(kJ mol^{-1})^{b}$	$(kJ mol^{-1})^{b}$	(kJ mol^{-1}) DFT + Bond Add. c
Pt from Ref 16 and Measured Here for Furfural						
phenol (site 1)	-29	4	0.53	41	91	130
phenol (site 2)	-9	0	0.40	21	71	76
benzaldehyde	-30.5	4.5	0.80	43 ^d	83	121/94
furfural	-26.1	0	0.89	26	84	95/92
benzyl alcohol	-33	5	0.86	32	99	159/128
cyclohexanol ^e	-17	0	0.66	-2	69	24/-3
			Rh			
phenol (site 1)	-26.3	0	0.62	39	89	86
phenol (site 2)	- 7	0	0.38	20	70	60
benzaldehyde (site 1)	-26.6	1.6	0.75	39^d	81	124
benzaldehyde (site 2)	-9	10	0.25	20^d	62	112
furfural	-25	0	0.82	25	83	88/66
benzyl alcohol (site 1)	-26.5	0	0.54	28	95	114
benzyl alcohol (site 2)	-8	10	0.36	9	76	104
cyclohexanol ^e	-3	0	0.63	- 7	63	-34/-65

"DFT-calculated values adjusted using the bond-additivity model are also included. ^bThe adsorption free energies are extracted from Figures 2 and 5. Heats of adsorption at standard coverage $\theta^{\circ} = 0.054$ are also listed based on conversions using the methodology described in the SI (Section S9). $-\Delta H^{\circ}_{ads,aq,\theta}$ refers to the heat of adsorption of solvated phenol, and $-\Delta H^{\circ}_{ads,aq,gas,\theta}$ refers to the aqueous-phase heat of adsorption of gas-phase phenol. $^{c}-\Delta H^{\circ}_{ads,aq,gas,\theta}$ is reported here from the values in Table S4 using the bond-additivity model. "Step" site values (site 1) correspond to (110) step calculations, and the "terrace" sites (site 2) correspond to (111) terraces. For molecules where two distinct adsorption sites were not found experimentally, (110) calculated values are listed first, followed by (111). d Heats of adsorption measured by solution calorimetry from ref 76 on Pt/C and Rh/C were 44 and 39 kJ mol $^{-1}$, respectively. "Cyclohexanol coverages did not reach saturation, so these values are estimated by using the same saturation coverage of phenol on site 1 for Rh (0.63 ML).

be a result of an erroneous treatment of water on the (100) steps in the model as described above for Pt.

The values of experimental adsorption free energies $(\Delta G_{\mathrm{ads,aq}, heta}^{\circ})$ from isotherm fitting using the procedure outlined in Section S6 are compiled in Table 1, along with the free energy of gas-phase organic adsorption in aqueous phase ($\Delta G_{ads,aq,gas,\theta}^{\circ}$), calculated from $\Delta G_{\mathrm{ads,aq},\theta}^{\circ}$ using Henry's law constant in Table S5. The adsorption values are also converted to enthalpies of gas-phase organic adsorption in aqueous phase $(\Delta H_{ads,aq,\sigma as,\theta}^{\circ})$ and aqueous organic adsorption enthalpies $(\Delta H_{\text{ads.aq.}\theta}^{\circ})$ following the method discussed in detail in Section S9 and outlined in Scheme S1. Briefly, the standard entropy of each gas-phase organic molecule is used to estimate the entropy of adsorption using a known correlation for many gas-phase molecules,6 allowing us to convert from $\Delta G_{ads,aq,gas,\theta}^{\circ}$ to $\Delta H_{ads,aq,gas,\theta}^{\circ}$. Although this accounts for the loss in entropy from the gasphase organic adsorption, we assume that the displaced water layer has the same entropy, i.e., that the water layer on top of the adsorbed organic has the same structural order as the water layer on top of the metal surface. This assumption of invariant entropy from water is supported by the close agreement between aqueous-phase calorimetry of benzaldehyde on both Pt/C and Rh/C compared to the enthalpies extracted here using this method. The assumption that the water layer maintains the same entropy could be tested by measuring $\Delta G^{\circ}_{\mathrm{ads,aq}, heta}$ as a function of temperature and constructing a van't Hoff plot so that this approximation is not required. If there was an increase in entropy from the water being displaced (i.e., water on the adsorbed organic has higher entropy than water adsorbed on the metal), the enthalpies of adsorption would be more positive than reported here, but the effect is estimated to not be more than 11 kJ mol-1.17

Difference in Gas-Phase and Aqueous-Phase Adsorption Energies of Phenol. Here, we compare our experimentally measured aqueous-phase heats of adsorption $(-\Delta H_{\mathrm{ads,aq,gas,}\theta}^{\circ})$ of phenol on both $\mathrm{Pt}(111)^{16,17}$ and $\mathrm{Rh}(111)$ with DFT-computed values in the gas phase and aqueous phase. The data in Figure 3 shows computed gas-phase heats of adsorption $(-\Delta H_{\mathrm{ads,aq,gas,}\theta}^{\circ})$ and aqueous-phase heats of adsorption $(-\Delta H_{\mathrm{ads,aq,gas,}\theta}^{\circ})$ calculated using implicit solvation, the bond-additivity approach, and experimental isotherm fitting. Our gas-phase DFT calculations for phenol heat of adsorption on $\mathrm{Pt}(111)$ agree with low-coverage values measured by

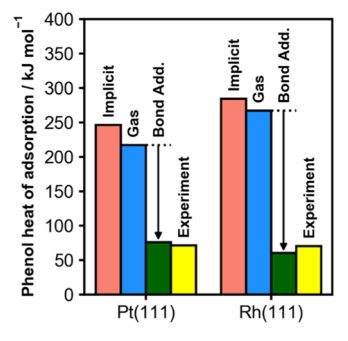


Figure 3. DFT-computed heats of adsorption in implicit solvent (orange), gas phase (blue), and aqueous phase using a bond-additivity model to correct the gas-phase calculation for solvation and water displacement at the metal interface (green). Experimentally derived heats of adsorption for gas-phase phenol on the metal in the aqueous phase for site 2, attributed to Pt(111) and Rh(111) terraces, are shown in yellow. Abbreviations: bond additivity = Bond Add.

ultrahigh vacuum calorimetry. Phenol is calculated to adsorb \sim 50 kJ mol⁻¹ stronger on Rh(111) compared with that on Pt(111) in the gas phase, but the experimental measurements show that both Rh(111) and Pt(111) adsorb phenol with similar and weaker strength in the aqueous phase.

Heats of adsorption computed using implicit solvation predict that phenol should adsorb stronger than in the gas phase on Pt and Rh and overpredict adsorption strengths by at least 100 kJ mol⁻¹ compared with the experiment. Here, calculations using only implicit solvation predict that phenol binds 29 kJ mol-1 stronger on Pt(111) in the aqueous phase compared with that of the gas phase, which is consistent with the 25 kJ mol⁻¹ increase in phenol binding strength previously reported using an implicit solvation model.⁴⁷ Past work that treated water explicitly reported the aqueous-phase adsorption enthalpy of a gas-phase phenol molecule to be 37 kJ mol⁻¹ more exothermic than in the gas phase. 45 Implicit and explicit solvent calculations that model water surrounding the organic but not displaced from the surface yield far more exothermic adsorption enthalpies than our equilibrated adsorption measurements and even calorimetry values. Reparameterizing the cavity of the VASPsol implicit solvent model for aromatic molecule adsorption may greatly improve the predicted heats of adsorption relative to our bondadditivity model predictions and experimental measurements. Also, DFT-calculated adsorption energies that account for displacement of adsorbed water from a metal surface 18 have not been compared directly with experimental values. The consequence of these significantly stronger adsorption energies would be a many orders of magnitude error in adsorption equilibrium constants, which are used for catalysis in trying to predict or understand surface coverages (e.g., through an LH reaction or other microkinetic model).

The bond-additivity model (eq 2) corrects the DFT-predicted gas-phase adsorption enthalpies for solvation and water displacement at the metal interface upon organic adsorption, bringing the predictions into much closer agreement with the experiment for phenol adsorption on Pt(111) and Rh(111). The bond-additivity model here does not account for the differences in the potential of zero charge (PZC) between Pt(111) and Rh(111), which could affect the metal surface charge and thus the water adsorption layer. The PZCs of the (111) facets of Pt and Rh in 0.1 M $_2$ SO₄ are much different (0.3 V on Pt(111) $_2$ 67,68 and 0.1 V on Rh(111) vs RHE).69 Accounting for this effect would further improve the accuracy of this model.

As previously discussed for Pt, ¹⁷ the difference in gas-phase and aqueous-phase adsorption is mainly attributed to the fact that in aqueous phase, organics must displace water adsorbed to the metal surface. This has been described qualitatively by Gileadi⁷⁰ and Bockris, ⁶⁴ but used quantitatively in recent work since we now know the number of water molecules displaced by phenol and the enthalpy associated with those adsorbed waters. For example, a phenol molecule adsorbing on Pt(111) surface in aqueous phase displaces approximately 6.5 water molecules, based on the footprint of adsorbed phenol on Pt⁵³ and saturation coverage of water on Pt. ⁵² Since Pt(111) has been recently shown to be the active facet for phenol hydrogenation, ¹⁰ it is important to understand how the presence of solvent/water impacts the effective adsorption strength of phenol on this facet.

The similarity between phenol adsorption on Rh and Pt in the aqueous phase is primarily caused by the stronger water adsorption on Rh than on Pt, as calculated here and in ref 71. Our DFT-calculated water/Rh(111) adsorption energy (-52 kJ

mol⁻¹) is stronger than water/Pt(111) (-39 kJ mol⁻¹) in the gas phase, consistent with temperature-programmed desorption experiments where water desorption on Rh(111) is observed at higher temperatures than on Pt(111).⁷² Water adsorption energies on other surfaces are included in Table S4. We assume that the phenol "footprint" is similar to Rh and Pt⁵³ and that *n* from eq 2 is the same for the two metals. This assumption is supported by the similar adsorption geometries (Figures S5 and S6) and metal surface area covered by phenol on Rh and Pt (0.60 nm² for Pt and 0.56 nm² for Rh) from our calculations. Thus, the stronger water adsorption on Rh offsets the stronger gas-phase phenol adsorption energy, resulting in comparable aqueous-phase adsorption energies.

Impact of Other Oxygenated Aromatics and Organics on the Underpotential Deposition of Hydrogen on Rh. Besides phenol, other oxygenated aromatics and organics (i.e., benzaldehyde, furfural, benzyl alcohol, cyclohexanol) tested here also compete with hydrogen for adsorption sites on Rh, as seen in Figure 4. Consequently, we can broadly apply the CV

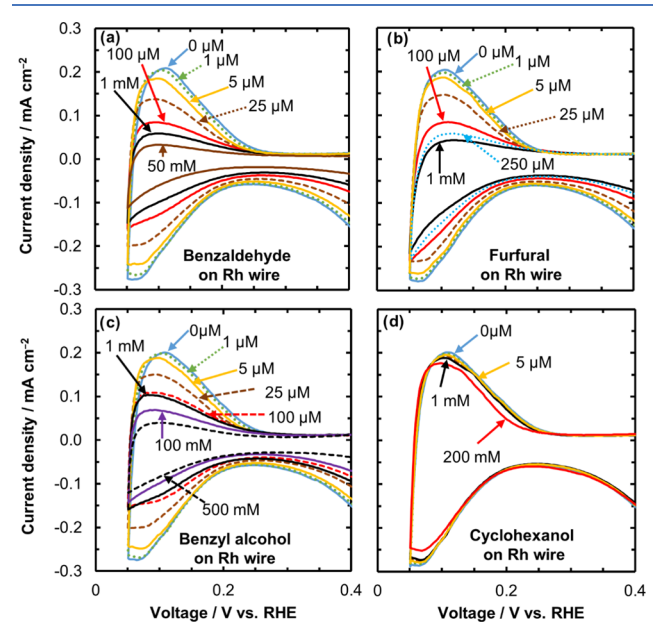


Figure 4. Cyclic voltammograms in the H_{upd} region with an increasing bulk organic concentration on a Rh wire for (a) benzaldehyde, (b) furfural, (c) benzyl alcohol, and (d) cyclohexanol. Experiments were carried out in a 100 mM acetate buffer supporting electrolyte (pH 5) at 298 K and using a 100 mV s⁻¹ scan rate. The adsorbed organic competes with H* for sites, hence the drop in H_{upd} charge indicated by the reduced current density with increasing organic concentration.

technique to extract adsorption energies of organics in the aqueous phase provided that in the H_{upd} potential window the adsorbed organic and H^* adsorb and desorb reversibly. The drop in the H_{upd} peaks with individual organic concentration varies in the order of furfural > benzaldehyde > phenol > benzyl alcohol \gg cyclohexanol. Cyclohexanol in particular has a much lower impact on the H_{upd} than the other organics, even at 200 mM.

Similar to the reversibility of $H_{\rm upd}$ discussed above for phenol, the $H_{\rm upd}$ charges in the cathodic and anodic directions in the presence of benzaldehyde, benzyl alcohol, and cyclohexanol are the same, implying reversible $H_{\rm upd}$; however, furfural $H_{\rm upd}$ (Figure 4b) became less reversible with increasing furfural concentration on Pt and Rh (Figures S7 and S8). With

increasing furfural concentration, a larger portion of the adsorbed hydrogen is not desorbed in the H_{upd} region (i.e., the difference in H_{upd} adsorption and desorption charges increases). This irreversible reduction current is also seen at higher furfural concentrations. 73 This behavior does not seem to be due to a catalytic reaction because the difference in H_{upd} adsorption and desorption charges was independent of scan rate (Figure S8c,d). Thus, one possibility for the irreversible H_{upd} reduction in the presence of furfural may be that H* partially hydrogenates the adsorbed furfural species, but complete furfural hydrogenation and desorption do not occur in this potential region. Recent studies have shown that furfural may also decarbonylate at potentials just positive of the H_{und} region, forming strongly adsorbed CO, adsorbed furyl fragments, and adsorbed H. 73,74 In this case, the irreversible reduction current we observe here may be related to the reduction or reaction of adsorbed furyl to furan, but without furan desorption that would allow catalytic turnover.

Adsorption Energies of Furfural, Benzaldehyde, Benzyl Alcohol, and Cyclohexanol on Rh. Using the data in Figure 4, the fraction of H_{upd} inhibited by the organics is shown in Figure 5, with specified points testing the reversibility of the adsorption process indicated by open symbols. The data in Figure S4 contains CVs used to test the reversibility of all organics tested here, except for cyclohexanol that did not adsorb at appreciable coverages. The adsorption free energies of these organics were extracted the same way as was done for phenol.

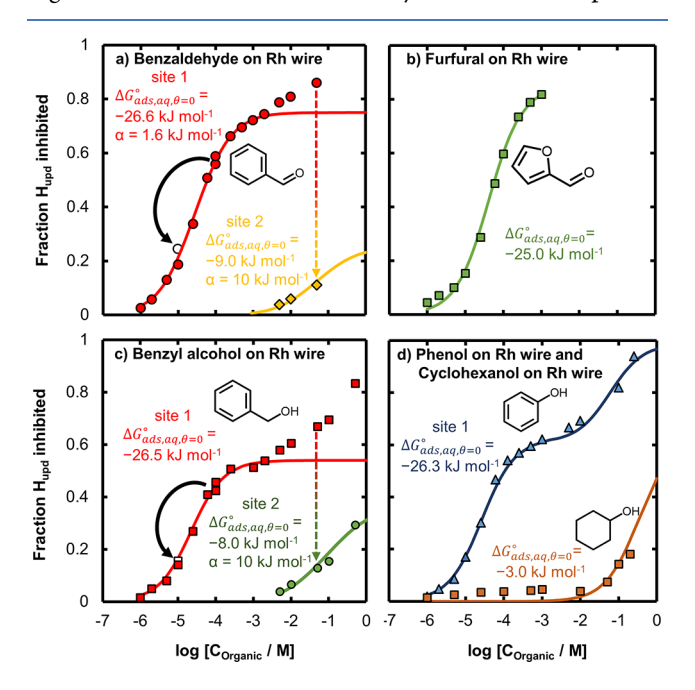


Figure 5. Adsorption isotherms of (a) benzaldehyde, (b) furfural, (c) benzyl alcohol, and (d) phenol on Rh wire and cyclohexanol on Rh wire. The data points were obtained from the fraction of H_{upd} inhibited on Rh by the different organics from Figure 4 at various organic concentrations. The values for phenol in (d) are from Figure 2b and are compared directly to the nonaromatic cyclohexanol values taken in a separate experiment to show the effect of the aromatic ring. A Temkin isotherm model was used to fit the data and extract the adsorption free energies. Benzaldehyde, phenol, and benzyl alcohol isotherms are divided into two sites for fitting. Furfural does not show a two-site adsorption behavior as seen for phenol. Dilution is shown by the solid arrows to test the reversibility of organic adsorption. New measurements after dilution are denoted by open symbols.

The two-site behavior seen for phenol on Rh is not observed for furfural and cyclohexanol. We deduce that furfural does not adsorb differently on the individual Rh facets as opposed to phenol, benzyl alcohol, and benzaldehyde, which adsorb on distinct Rh sites (attributed to stronger adsorption on steps and weaker adsorption on terraces). This may also be a result of furfural decarbonylating upon adsorption, as discussed earlier. Thus, the extracted adsorption energies of furfural without a two-site adsorption behavior are an average over the different sites. For cyclohexanol, the adsorption is not strong enough to reach sufficiently high coverages where adsorption on a second site may be seen. Further coverage increases were limited by the solubility of cyclohexanol. The fraction of H_{upd} inhibited at 1 mM cyclohexanol concentration, shown in Figure 5d, is less than 5%, whereas for other organics (Figure 5), greater than 50% organic coverage was achieved at 1 mM. Our DFT calculations also indicate that cyclohexanol adsorption is weaker on Pt and Rh than aromatic adsorption. As the main difference between the phenol and cyclohexanol is the aromatic ring, the weaker adsorption of cyclohexanol (Figure 5d) is consistent with the idea that the adsorption of aromatics on a transition metal arises from the interaction between the aromatic π electron system and the metal d-band.⁷⁵ The measured adsorption energies of the model compounds are included in Table 1, converted between free energies and enthalpies as discussed in Section S9 of the SI. Table 1 also includes the adsorption energies from calculations using DFT and adjusting using the bond-additivity model.

Comparing Experiments with Implicit Solvent and Bond-Additivity Calculations. The aqueous-phase heats of adsorption from experiments on Rh increase in the order of benzaldehyde > phenol > benzyl alcohol > furfural ≫ cyclohexanol, which has the same trend as Pt in aqueous phase. 16 Furfural adsorption on Pt was not previously measured in ref 16 but is reported here (H_{upd} and adsorption isotherm are in Figure S9). The heat of adsorption for benzaldehyde on site 1 of Rh (39 kJ mol⁻¹) obtained here from the isotherm fitting is the same as the value determined from solution calorimetry of benzaldehyde on Rh/C (39 kJ mol⁻¹),⁷⁶ supporting the accuracy of this technique for estimating adsorption energies on metal surfaces. The exact order of the heats of adsorption for the aromatics differs between experiment and our computationally predicted energies (Table 1), yet this is unsurprising given the small variation in heats of adsorption on a given site, which is well within the expected accuracy of DFT-based predictions, and the assumptions/estimates of the number of waters displaced and its impact on the predicted adsorption energies. Nevertheless, the much stronger adsorption of the aromatic molecules compared with the more weakly adsorbing cyclohexanol is captured by our computational results.

The differences between experimental and predicted heats of adsorption for all five organics studied here are shown in Figure 6. Heats of adsorption were also predicted using the optB88-vdw functional, 77,78 which has been used to predict accurate gasphase adsorption energies of phenol on Pt(111), 79 though we find no qualitative differences between using the optB88-vdw functional and PBE-D3 (see Figure S12 of the SI for comparison). The heat of adsorption of each molecule on the (110) step and the (111) terrace is calculated in the gas phase and in the aqueous phase using either DFT with implicit solvent or the bond-additivity model. Here, we use the (110) step to compare the experimental site 1 and the (111) terrace to compare site 2. The triangles for phenol in Figure 6 correspond to the difference between the values shown in Figure 3.

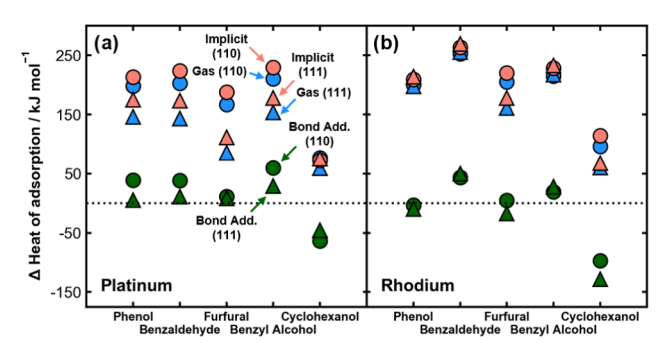


Figure 6. Calculated heats of adsorption using the PBE-D3 functional referenced to experimental heats of adsorption for organics using different methods. Calculations on (110) steps are compared to site 1 and (111) facets are compared to site 2. (a) Pt(110) step and Pt(111) terrace differences between theory and experiment; (b) Rh(110) step and Rh(111) terrace differences. Heats of adsorption are calculated in the gas phase and in the aqueous phase using an implicit solvent model or a bond-additivity model (Bond Add.). Calculated enthalpies on the (111) terrace and (110) step were referenced to the same experimental enthalpy when two distinct adsorption sites were not extracted from the isotherms. Values greater than zero indicate that adsorption is predicted by DFT to be stronger than the experiment, whereas values less than zero indicate that adsorption is predicted by DFT to be weaker. Experimental values and Bond Add. values are shown in Table 1, and all computational values are shown in Table S4.

Generally, the energy of solvating organics and the penalty of displacing adsorbed water, which is explicitly accounted for in the bond-additivity model, result in a drastic reduction in the heats of adsorption of the organics in the aqueous phase compared with that in the gas phase.

For all organics, a large difference between the gas-phase and experimental heats of adsorption is observed, indicating that gasphase DFT predicts adsorption to be much stronger than what is observed experimentally in the aqueous phase. Similarly, DFT with implicit solvent predicts the adsorption of the organics to be much stronger than what is experimentally measured. The heats of adsorption predicted using the bond-additivity model, however, are much closer to experimental values for all organics, with cyclohexanol as an exception. Since cyclohexanol adsorbs so weakly, we are unable to get a saturation coverage; hence, the isotherm fit is poor and the extracted aqueous values may not be accurate. Furthermore, because cyclohexanol already binds weakly in the gas phase compared with the aromatics, it may have an insufficient driving force to displace as many water molecules as the aromatics.

The number of water molecules displaced by each organic molecule (used for bond additivity) from each surface was chosen based on an estimated saturation coverage of each organic and an approximate coverage of water (Figure S10 and Table S6). Unsurprisingly, the closest agreement between bond-additivity calculations and the experimental values is for (111) terraces, where UHV work has given a more accurate understanding of the footprint of the adsorbed organic and hence the number of displaced waters. Ultimately, the data in Table 1 and Figure 6 show that the adsorption enthalpies of the organics in aqueous phase are greatly reduced by the presence of water compared with gas-phase adsorption enthalpies and that closer agreement with experimental measurements in aqueous phase is obtained with the bond-additivity model.

Consequences of Weaker Effective Organic Adsorption on Pt and Rh on Hydrogenation Rates. The comparable free energies of adsorption of phenol and

benzaldehyde on Rh and Pt wires in aqueous phase may explain why there is considerable similarity in the Rh/C and Pt/C activities for both aqueous-phase thermal and electrocatalytic hydrogenation of these molecules. Aqueous-phase hydrogenation of phenol and benzaldehyde on Pt/C and Rh/C can be described using a Langmuir-Hinshelwood mechanism with a surface reaction rate-determining step, 9,76 so the adsorption energies of the organic and of hydrogen should play a key role in the observed kinetics. In particular, the adsorption energies of the reactants and intermediates will dictate the surface coverages when adsorption/desorption is fast compared to the surface reaction; thus, these adsorption energies will control the reaction orders. The adsorption energies will also impact the TOF, both through the surface coverages and the activation energies. Phenol has similar TOFs and reaction orders for hydrogenation of the aromatic ring on Pt/C and Rh/C.8,14 Benzaldehyde also shows comparable hydrogenation TOFs and reaction orders for the aldehyde group on Pt/C and Rh/C.⁷⁶ Pt and Rh have similar effective activation energies for phenol^{8,9} and benzaldehyde, 76 with Rh having a slightly lower (~4 to 6 kJ mol⁻¹) effective activation energy for both reactions.

The similar hydrogen adsorption energies of Pt and Rh,80 combined with the above evidence for aqueous-phase hydrogenation, imply that there are no major differences in the organic adsorption energy on Pt and Rh. This observation is inconsistent with the different organic adsorption strengths in gas phase (e.g., phenol adsorbs 50 kJ mol⁻¹ more strongly on Rh(111) than on Pt(111)). However, the similar aqueous adsorption strengths for Pt and Rh in this work agree qualitatively with the observed catalytic activity for phenol and benzaldehyde hydrogenation. In addition, the much lower adsorption energy for phenol and benzaldehyde in the aqueous phase explains why these reactions can proceed at room temperature, whereas in gas phase the adsorption energy would be too strong for appreciable reaction, and desorption may be rate-limiting, as opposed to the surface reaction being rate-limiting in aqueous phase. The adsorption equilibrium constant for phenol on Pt(111) using the bondadditivity model¹⁷ in fact matches closely to the adsorption equilibrium constant for phenol hydrogenation on Pt/C, whereas the adsorption constant from gas-phase or implicit solvent calculations is more than 30 orders of magnitude too large. The large difference in gas-phase and aqueous-phase adsorption energies highlights the importance of understanding adsorption in aqueous phase for catalysis, which we show can be approximated using gas-phase calculations coupled with the bond-additivity model. Although this method would enable more accurate estimates of coverage and adsorption/desorption, it would not account for solvent effects in preferentially stabilizing the transition state or identifying new reaction mechanisms that require interaction with the solvent.

CONCLUSIONS

Generally, we find that organics bind weaker in the aqueous phase compared to the gas phase on Pt and Rh. This observation is well explained by a bond-additivity model that accounts for the large enthalpic penalty for the displacement of multiple water molecules by the organics from the water/metal interface. Using this model, we predicted adsorption energies in aqueous phase from gas-phase calculations, which match qualitatively with experiments. As a result of this water displacement enthalpy, phenol and other organics adsorb with similar strength on Pt and Rh in aqueous phase despite the considerable difference in their gas-phase adsorption enthalpies.

Although for surface reactions, this weaker adsorption in aqueous phase may apply to the energies of adsorbed products, intermediates, and transition states equally relative to the adsorbed reactant species and thus may not greatly change catalytic barriers, the weakening of adsorption energies has important consequences in understanding adsorption/desorption, coverages, and TOFs. These results help explain how aromatics such as furfural, benzaldehyde, and phenol, which bind so strongly to metals in the gas phase $(200-250 \text{ kJ mol}^{-1})$, can be hydrogenated even at room temperature in the presence of water. Additionally, these findings show how computational techniques can be used to predict and rationalize how solvents tune the adsorption on metal surfaces. Understanding how solvents impact the adsorption can enable the control of condensed-phase catalytic rates through the selection of the solvent environment.

ASSOCIATED CONTENT

Solution Supporting Information

The Supporting Information is available free of charge at https://pubs.acs.org/doi/10.1021/acscatal.0c00803.

Details of experimental cyclic voltammograms, reversibility of $H_{\rm upd}$ with organics, isotherm fitting, procedure for extracting aqueous enthalpies, computational geometries and adsorption energies, and discussion of the bond-additivity model (PDF)

AUTHOR INFORMATION

Corresponding Authors

Bryan R. Goldsmith — Department of Chemical Engineering and Catalysis Science and Technology Institute, University of Michigan, Ann Arbor, Michigan 48109 2136, United States; orcid.org/0000-0003-1264-8018; Email: bgoldsm@umich.edu

Nirala Singh — Department of Chemical Engineering and Catalysis Science and Technology Institute, University of Michigan, Ann Arbor, Michigan 48109 2136, United States; orcid.org/0000-0003-0389-3927; Email: snirala@umich.edu

Authors

James Akinola — Department of Chemical Engineering and Catalysis Science and Technology Institute, University of Michigan, Ann Arbor, Michigan 48109 2136, United States;
[®] orcid.org/0000-0002-8526-865X

Isaiah Barth – Department of Chemical Engineering and Catalysis Science and Technology Institute, University of Michigan, Ann Arbor, Michigan 48109 2136, United States; ◎ orcid.org/ 0000-0002-3052-0467

Complete contact information is available at: https://pubs.acs.org/10.1021/acscatal.0c00803

Author Contributions

The manuscript was written through contributions of all authors. All authors have given approval to the final version of the manuscript.

Funding

This material is based upon the work supported by the National Science Foundation under Grant No. #1919444.

Notes

The authors declare no competing financial interest.

ACKNOWLEDGMENTS

This research used resources of the National Energy Research Scientific Computing Center (NERSC), a U.S. Department of Energy Office of Science User Facility operated under Contract No. DE-AC02-05CH11231.

ABBREVIATIONS USED

Bond Add., bond additivity; CV, cyclic voltammetry or cyclic voltammogram; DFT, density functional theory; H_{upd}, hydrogen underpotential deposition; PZC, potential of zero charge; RHE, reversible hydrogen electrode; VASP, Vienna ab initio simulation package; ML, monolayer; LH, Langmuir—Hinshelwood

REFERENCES

- (1) EIA, U.S. Energy Information Administration. *Annual Energy Outlook 2018 with Projections to 2050*; US Energy Information Administration, Office of Energy Analysis, U.S. Department of Energy: Washington, DC 20585, 2019.
- (2) Czernik, S.; Bridgwater, A. V. Overview of Applications of Biomass Fast Pyrolysis Oil. *Energy Fuels* **2004**, *18*, 590–598.
- (3) Zhang, Q.; Chang, J.; Wang, T.; Xu, Y. Review of Biomass Pyrolysis Oil Properties and Upgrading Research. *Energy Convers. Manag.* **2007**, 48, 87–92.
- (4) Scott, D. S.; Piskorz, J.; Radlein, D. Liquid Products from the Continuous Flash Pyrolysis of Biomass. *Ind. Eng. Chem. Process Des. Dev.* 1985, 24, 581–588.
- (5) Carneiro, J.; Nikolla, E. Electrochemical Conversion of Biomass-Based Oxygenated Compounds. *Annu. Rev. Chem. Biomol. Eng.* **2019**, *10*, 85–104.
- (6) Furimsky, E. Catalytic Hydrodeoxygenation. *Appl. Catal., A* **2000**, 199, 147–190.
- (7) Carey, S. J.; Zhao, W.; Mao, Z.; Campbell, C. T. Energetics of Adsorbed Phenol on Ni(111) and Pt(111) by Calorimetry. *J. Phys. Chem. C* 2019, 123, 7627–7632.
- (8) Singh, N.; Song, Y.; Gutiérrez, O. Y.; Camaioni, D. M.; Campbell, C. T.; Lercher, J. A. Electrocatalytic Hydrogenation of Phenol over Platinum and Rhodium: Unexpected Temperature Effects Resolved. *ACS Catal.* **2016**, *6*, 7466–7470.
- (9) Song, Y.; Gutiérrez, O. Y.; Herranz, J.; Lercher, J. A. Aqueous Phase Electrocatalysis and Thermal Catalysis for the Hydrogenation of Phenol at Mild Conditions. *Appl. Catal., B* **2016**, *182*, 236–246.
- (10) Sanyal, U.; Song, Y.; Singh, N.; Fulton, J. L.; Herranz, J.; Jentys, A.; Gutiérrez, O. Y.; Lercher, J. A. Structure Sensitivity in Hydrogenation Reactions on Pt/C in Aqueous-phase. *ChemCatChem* **2019**, 11, 575–582.
- (11) Sasaki, K.; Kunai, A.; Harada, J.; Nakabori, S. Electrolytic Hydrogenation of Phenols in Aqueous Acid Solutions. *Electrochim. Acta* **1983**, *28*, *671*–*674*.
- (12) Singh, N.; Lee, M. S.; Akhade, S. A.; Cheng, G.; Camaioni, D. M.; Gutiérrez, O. Y.; Glezakou, V. A.; Rousseau, R.; Lercher, J. A.; Campbell, C. T. Impact of pH on Aqueous-Phase Phenol Hydrogenation Catalyzed by Carbon-Supported Pt and Rh. *ACS Catal.* **2019**, *9*, 1120–1128.
- (13) Honkela, M. L.; Björk, J.; Persson, M. Computational Study of the Adsorption and Dissociation of Phenol on Pt and Rh Surfaces. *Phys. Chem. Chem. Phys.* **2012**, *14*, 5849–5854.
- (14) Song, Y.; Chia, S. H.; Sanyal, U.; Gutiérrez, O. Y.; Lercher, J. A. Integrated Catalytic and Electrocatalytic Conversion of Substituted Phenols and Diaryl Ethers. *J. Catal.* **2016**, *344*, 263–272.
- (15) Werpy, T.; Petersen, G. Top Value Added Chemicals from Biomass: Volume I -- Results of Screening for Potential Candidates from Sugars and Synthesis Gas; Golden, CO (United States), 2004; pp 6–16.
- (16) Singh, N.; Sanyal, U.; Fulton, J. L.; Gutiérrez, O. Y.; Lercher, J. A.; Campbell, C. T. Quantifying Adsorption of Organic Molecules on Platinum in Aqueous Phase by Hydrogen Site Blocking and in Situ X-Ray Absorption Spectroscopy. ACS Catal. 2019, 9, 6869–6881.

- (17) Singh, N.; Campbell, C. T. A Simple Bond-Additivity Model Explains Large Decreases in Heats of Adsorption in Solvents Versus Gas Phase: A Case Study with Phenol on Pt(111) in Water. ACS Catal. **2019**, *9*, 8116–8127.
- (18) Kristoffersen, H. H.; Shea, J. E.; Metiu, H. Catechol and HCl Adsorption on $TiO_2(110)$ in Vacuum and at the Water- TiO_2 Interface. *J. Phys. Chem. Lett.* **2015**, *6*, 2277–2281.
- (19) Łosiewicz, B.; Jurczakowski, R.; Lasia, A. Kinetics of Hydrogen Underpotential Deposition at Polycrystalline Rhodium in Acidic Solutions. *Electrochim. Acta* **2011**, *56*, 5746–5753.
- (20) Zolfaghari, A.; Villiard, F.; Chayer, M.; Jerkiewicz, G. Hydrogen Adsorption on Pt and Rh Electrodes and Blocking of Adsorption Sites by Chemisorbed Sulfur. *J. Alloys Compd.* **1997**, 253–254, 481–487.
- (21) Jerkiewicz, G.; Zolfaghari, A. Comparison of Hydrogen Electroadsorption from the Electrolyte with Hydrogen Adsorption from the Gas Phase. *J. Electrochem. Soc.* **1996**, *143*, 1240–1248.
- (22) DeBlois, M.; Lessard, J.; Jerkiewicz, G. Influence of Benzene on the H_{upd} and Anion Adsorption on Pt(110), Pt(100) and Pt(111) Electrodes in Aqueous H₂SO₄. Electrochim. Acta **2005**, 50, 3517–3523.
- (23) Obradović, M. D.; Lessard, J.; Jerkiewicz, G. Cyclic-Voltammetry Behavior of Pt(111) in Aqueous $HClO_4 + C_6H_6$: Influence of C_6H_6 Concentration, Scan Rate and Temperature. *J. Electroanal. Chem.* **2010**, 649, 248–256.
- (24) Gasparotto, L. H. S.; Gomes, J. F.; Tremiliosi-Filho, G. Cyclic-Voltammetry Characteristics of Poly(Vinyl Pyrrolidone) (PVP) on Single-Crystal Pt Surfaces in Aqueous H₂SO₄. *J. Electroanal. Chem.* **2011**, *663*, 48–51.
- (25) Lam, C. H.; Das, S.; Erickson, N. C.; Hyzer, C. D.; Garedew, M.; Anderson, J. E.; Wallington, T. J.; Tamor, M. A.; Jackson, J. E.; Saffron, C. M. Towards Sustainable Hydrocarbon Fuels with Biomass Fast Pyrolysis Oil and Electrocatalytic Upgrading. *Sustainable Energy Fuels* **2017**, *1*, 258–266.
- (26) Wieckowski, A.; Sobrowski, J.; Zelenay, P.; Franaszczuk, K. Adsorption of Acetic Acid on Platinum, Gold and Rhodium Electrodes. *Electrochim. Acta* **1981**, 26, 1111–1119.
- (27) Garrone, E.; Bolis, V.; Fubini, B.; Morterra, C. Thermodynamic and Spectroscopic Characterization of Heterogeneity among Adsorption Sites: CO on Anatase at Ambient Temperature. *Langmuir* **1989**, *5*, 892–899
- (28) Vassiliev, Y. B.; Bagotzky, V. S.; Khazova, O. A.; Cherny, V. V.; Meretsky, A. M. Mechanism of Adsorption, Electroreduction and Hydrogenation of Compounds with Ethylenic Bonds on Platinum and Rhodium: Part I. Kinetics of Adsorption and Electroreduction. *J. Electroanal. Chem. Interfacial Electrochem.* 1979, 98, 253–272.
- (29) Singh, N.; Sanyal, U.; Ruehl, G.; Gutiérrez, O. Y.; Camaioni, D. M.; Fulton, J. L.; Lercher, J. A.; Campbell, C. T.; Stoerzinger, K. A. Aqueous Phase Catalytic and Electrocatalytic Hydrogenation of Phenol and Benzaldehyde over Platinum Group Metals. *J. Catal.* **2020**, 382, 372–384
- (30) Bard, A. J.; Faulkner, L. R. Electrochemical Methods: Fundamentals and Applications; Wiley: New York, 2001; Vol. 2, pp 554–556.
- (31) Electrosorption; Gileadi, E., Ed.; Springer Science & Business Media, 2012; p 93.
- (32) Bockris, J. O. M.; Green, M.; Swinkels, D. A. J. Adsorption of Naphthalene on Solid Metal Electrodes. *J. Electrochem. Soc.* **1964**, *111*, 743–748.
- (33) Kresse, G.; Furthmüller, J. Efficiency of Ab-Initio Total Energy Calculations for Metals and Semiconductors Using a Plane-Wave Basis Set. *Comput. Mater. Sci.* **1996**, *6*, 15–50.
- (34) Kresse, G.; Furthmüller, J. Efficient Iterative Schemes for Ab Initio Total-Energy Calculations Using a Plane-Wave Basis Set. *Phys. Rev. B* **1996**, *54*, 11169–11186.
- (35) Goerigk, L.; Grimme, S. A Thorough Benchmark of Density Functional Methods for General Main Group Thermochemistry, Kinetics, and Noncovalent Interactions. *Phys. Chem. Chem. Phys.* **2011**, 13, 6670–6688.
- (36) Gautier, S.; Steinmann, S. N.; Michel, C.; Fleurat-Lessard, P.; Sautet, P. Molecular Adsorption at Pt(111). How Accurate Are DFT Functionals? *Phys. Chem. Chem. Phys.* **2015**, *17*, 28921–28930.

- (37) Grimme, S.; Antony, J.; Ehrlich, S.; Krieg, H. A Consistent and Accurate Ab Initio Parametrization of Density Functional Dispersion Correction (DFT-D) for the 94 Elements H-Pu. *J. Chem. Phys.* **2010**, 132, No. 154104.
- (38) Perdew, J. P.; Burke, K.; Ernzerhof, M. Generalized Gradient Approximation Made Simple. *Phys. Rev. Lett.* **1996**, *77*, 3865–3868.
- (39) Blöchl, P. E. Projector Augmented-Wave Method. *Phys. Rev. B* **1994**, *50*, 17953–17979.
- (40) Haas, P.; Tran, F.; Blaha, P. Calculation of the Lattice Constant of Solids with Semilocal Functionals. *Phys. Rev. B* **2009**, 79, No. 085104.
- (41) Kittel, C. Introduction to Solid State Physics, 8th ed.; Wiley: New Jersey, 2004; p 20.
- (42) Saleheen, M.; Heyden, A. Liquid-Phase Modeling in Heterogeneous Catalysis. ACS Catal. 2018, 8, 2188–2194.
- (43) Sievers, C.; Noda, Y.; Qi, L.; Albuquerque, E. M.; Rioux, R. M.; Scott, S. L. Phenomena Affecting Catalytic Reactions at Solid—Liquid Interfaces. *ACS Catal.* **2016**, *6*, 8286—8307.
- (44) Bodenschatz, C. J.; Sarupria, S.; Getman, R. B. Molecular-Level Details about Liquid H₂O Interactions with CO and Sugar Alcohol Adsorbates on Pt(111) Calculated Using Density Functional Theory and Molecular Dynamics. *J. Phys. Chem. C* **2015**, *119*, 13642–13651.
- (45) Yoon, Y.; Rousseau, R.; Weber, R. S.; Mei, D.; Lercher, J. A. First-Principles Study of Phenol Hydrogenation on Pt and Ni Catalysts in Aqueous Phase. *J. Am. Chem. Soc.* **2014**, *136*, 10287–10298.
- (46) Faheem, M.; Heyden, A. Hybrid Quantum Mechanics/ Molecular Mechanics Solvation Scheme for Computing Free Energies of Reactions at Metal—Water Interfaces. *J. Chem. Theory Comput.* **2014**, *10*, 3354—3368.
- (47) Iyemperumal, S. K.; Deskins, N. A. Evaluating Solvent Effects at the Aqueous/Pt(111) Interface. *ChemPhysChem* **2017**, *18*, 2171–2190.
- (48) Saleheen, M.; Verma, A. M.; Mamun, O.; Lu, J.; Heyden, A. Investigation of Solvent Effects on the Hydrodeoxygenation of Guaiacol over Ru Catalysts. *Catal. Sci. Technol.* **2019**, *9*, 6253–6273.
- (49) Mathew, K.; Sundararaman, R.; Letchworth-Weaver, K.; Arias, T. A.; Hennig, R. G. Implicit Solvation Model for Density-Functional Study of Nanocrystal Surfaces and Reaction Pathways. *J. Chem. Phys.* **2014**, *140*, No. 084106.
- (50) Mathew, K.; Kolluru, V. S. C.; Mula, S.; Steinmann, S. N.; Hennig, R. G. Implicit Self-Consistent Electrolyte Model in Plane-Wave Density-Functional Theory. *J. Chem. Phys* **2019**, *151*, No. 234101.
- (51) Rumptz, J. R.; Campbell, C. T. Adhesion Energies of Solvent Films to Pt(111) and Ni(111) Surfaces by Adsorption Calorimetry. *ACS Catal.* **2019**, *9*, 11819–11825.
- (52) Lew, W.; Crowe, M. C.; Karp, E.; Campbell, C. T. Energy of Molecularly Adsorbed Water on Clean Pt(111) and Pt(111) with Coadsorbed Oxygen by Calorimetry. *J. Phys. Chem. C* **2011**, *115*, 9164–9170.
- (53) Lu, F.; Salaita, G. N.; Laguren-Davidson, L.; Stern, D. A.; Wellner, E.; Frank, D. G.; Batina, N.; Zapien, D. C.; Walton, N.; Hubbard, A. T. Characterization of Hydroquinone and Related Compounds Adsorbed at Pt(111) from Aqueous Solutions: Electron Energy-Loss Spectroscopy, Auger Spectroscopy, LEED, and Cyclic Voltammetry. *Langmuir* 1988, 4, 637–646.
- (54) Farias, M. J. S.; Camara, G. A.; Feliu, J. M. Understanding the CO Preoxidation and the Intrinsic Catalytic Activity of Step Sites in Stepped Pt Surfaces in Acidic Medium. *J. Phys. Chem. C* **2015**, *119*, 20272–20282.
- (55) Souza-Garcia, J.; Climent, V.; Feliu, J. M. Voltammetric Characterization of Stepped Platinum Single Crystal Surfaces Vicinal to the (110) Pole. *Electrochem. Commun.* **2009**, *11*, 1515–1518.
- (56) Domke, K.; Herrero, E.; Rodes, A.; Feliu, J. M. Determination of the Potentials of Zero Total Charge of Pt(100) Stepped Surfaces in the $[01\overline{1}]$ Zone. Effect of the Step Density and Anion Adsorption. *J. Electroanal. Chem.* **2003**, 552, 115–128.
- (57) Arán-Ais, R. M.; Figueiredo, M. C.; Vidal-Iglesias, F. J.; Climent, V.; Herrero, E.; Feliu, J. M. On the Behavior of the Pt(100) and Vicinal Surfaces in Alkaline Media. *Electrochim. Acta* **2011**, *58*, 184–192.

- (58) Souza-Garcia, J.; Angelucci, C. A.; Climent, V.; Feliu, J. M. Electrochemical Features of Pt(S)[n(110) × (100)] Surfaces in Acidic Media. *Electrochem. Commun.* **2013**, *34*, 291–294.
- (59) Molodkina, E. B.; Danilov, A. I.; Feliu, J. M. Cu UPD at Pt(100) and Stepped Faces Pt(610), Pt(410) of Platinum Single Crystal Electrodes. *Russ. J. Electrochem.* **2016**, 52, 890–900.
- (60) Sasahara, A.; Tamura, H.; Tanaka, K. Catalytic Activity of Pt-Deposited Rh(110) Bimetallic Surface for NO + H₂ Reaction. *J. Phys. Chem. B* **1997**, *101*, 1186–1189.
- (61) Wasberg, M.; Hourani, M.; Wieckowski, A. Comparison of Voltammetry of Vacuum-Prepared Rh (100) and Rh (111) Electrodes. *J. Electroanal. Chem. Interfacial Electrochem.* **1990**, 278, 425–432.
- (62) Clavilier, J.; Wasberg, M.; Petit, M.; Klein, L. H. Detailed Analysis of the Voltammetry of Rh(111) in Perchloric Acid Solution. *J. Electroanal. Chem.* **1994**, 374, 123–131.
- (63) Hourani, M.; Wieckowski, A. Single Crystal Electrochemistry of Rhodium: Anion Effects and Order/Disorder Transitions of Clean and Silver Coated Rh (111) Surfaces. *J. Electroanal. Chem. Interfacial Electrochem.* **1988**, 244, 147–161.
- (64) Bockris, J. O.; Jeng, K. T. In-Situ Studies of Adsorption of Organic Compounds on Platinum Electrodes. *J. Electroanal. Chem.* **1992**, 330, 541–581.
- (65) McCrum, I. T.; Hickner, M. A.; Janik, M. J. First-Principles Calculation of Pt Surface Energies in an Electrochemical Environment: Thermodynamic Driving Forces for Surface Faceting and Nanoparticle Reconstruction. *Langmuir* 2017, 33, 7043–7052.
- (66) Campbell, C. T.; Sellers, J. R. V. The Entropies of Adsorbed Molecules. J. Am. Chem. Soc. 2012, 134, 18109—18115.
- (67) Weaver, M. J. Potentials of Zero Charge for Platinum(111)—Aqueous Interfaces: A Combined Assessment from In-Situ and Ultrahigh-Vacuum Measurements. *Langmuir* 1998, 14, 3932—3936.
- (68) Gómez, R.; Feliu, J. M.; Aldaz, A.; Weaver, M. J. Validity of Double-Layer Charge-Corrected Voltammetry for Assaying Carbon Monoxide Coverages on Ordered Transition Metals: Comparisons with Adlayer Structures in Electrochemical and Ultrahigh Vacuum Environments. Surf. Sci. 1998, 410, 48–61.
- (69) Xu, Q.; Linke, U.; Bujak, R.; Wandlowski, T. Preparation and Electrochemical Characterization of Low-Index Rhodium Single Crystal Electrodes in Sulfuric Acid. *Electrochim. Acta* **2009**, *54*, 5500–5521
- (70) Gileadi, E. Electrosorption of Uncharged Molecules on Solid Electrodes. *J. Electroanal. Chem.* **1966**, *11*, 137–151.
- (71) Meng, S.; Wang, E. G.; Gao, S. Water Adsorption on Metal Surfaces: A General Picture from Density Functional Theory Studies. *Phys. Rev. B* **2004**, *69*, No. 195404.
- (72) Wagner, F. T.; Moylan, T. E. A Comparison between Water Adsorbed on Rh(111) and Pt(111), with and without Predosed Oxygen. Surf. Sci. 1987, 191, 121–146.
- (73) Roman, A. M.; Hasse, J. C.; Medlin, J. W.; Holewinski, A. Elucidating Acidic Electro-Oxidation Pathways of Furfural on Platinum. ACS Catal. 2019, 9, 10305–10316.
- (74) Gong, L.; Agrawal, N.; Roman, A.; Holewinski, A.; Janik, M. J. Density Functional Theory Study of Furfural Electrochemical Oxidation on the Pt (1 1 1) Surface. *J. Catal.* **2019**, *373*, 322–335.
- (75) Jing, Z.; Whitten, J. L. The Adsorption of Benzene on Ni(111). *Surf. Sci.* **1991**, 250, 147–158.
- (76) Song, Y.; Sanyal, U.; Pangotra, D.; Holladay, J. D.; Camaioni, D. M.; Gutiérrez, O. Y.; Lercher, J. A. Hydrogenation of Benzaldehyde via Electrocatalysis and Thermal Catalysis on Carbon-Supported Metals. *J. Catal.* **2018**, 359, 68–75.
- (77) Klimeš, J.; Bowler, D. R.; Michaelides, A. Chemical Accuracy for the van Der Waals Density Functional. *J. Phys.: Condens. Matter* **2010**, 22, No. 022201.
- (78) Klimeš, J.; Bowler, D. R.; Michaelides, A. Van Der Waals Density Functionals Applied to Solids. *Phys. Rev. B* **2011**, *83*, No. 195131.
- (79) Jia, X.; An, W. Adsorption of Monocyclic Aromatics on Transition Metal Surfaces: Insight into Variation of Binding Strength from First-Principles. *J. Phys. Chem. C* **2018**, *122*, 21897–21909.

(80) Gorodetskii, V. V.; Nieuwenhuys, B. E.; Sachtler, W. M. H.; Boreskov, G. K. Adsorption of Hydrogen on Rhodium; Comparison with Hydrogen Adsorption on Platinum and Iridium. *Surf. Sci.* **1981**, 108, 225–234.